IJC
International Journal of Cancer

Preclinical evaluation of near-infrared (NIR) fluorescently labeled cetuximab as a potential tool for fluorescence-guided surgery

Mara Saccomano[1], Christian Dullin[2], Frauke Alves[1,2,3] and Joanna Napp[1,2,3]

[1] Department of Molecular Biology of Neuronal Signals, Max-Planck-Institute of Experimental Medicine, Göttingen, Germany
[2] Institute of Interventional and Diagnostic Radiology, University Medical Center Göttingen, Göttingen, Germany
[3] Department of Haematology and Medical Oncology, University Medical Center Göttingen, Göttingen, Germany

The high rate of recurrence in patients with pancreatic ductal adenocarcinoma (PDAC) could be reduced by supporting the surgeons in discriminating healthy from diseased tissues with intraoperative fluorescence-guidance. Here, we studied the suitability of Cetuximab, a therapeutic monoclonal antibody targeting the human epidermal growth factor receptor (EGFR), near-infrared (NIR) fluorescently labeled as a new tool for fluorescence-guided surgery. Distribution and binding of systemically injected Cetuximab Alexa Fluor 647 conjugate (Cetux-Alexa-647) and the co-injected control human IgG Alexa Fluor 750 conjugate (hIgG-Alexa-750) was studied over 48 h by NIR fluorescence imaging in mice bearing human orthotopic AsPC-1 and MIA PaCa-2 PDAC tumors. Cetux-Alexa-647, but not the control hIgG-Alexa-750 fluorescence, was specifically detected *in vivo* in both primary pancreatic tumors with maximum fluorescence intensities at 24 h, and in metastases of AsPC-1 tumors as small as 1 mm. Lifetime analysis and NIR fluorescence microscopy of tumor sections confirmed the binding specificity of Cetux-Alexa-647 to PDAC cells. Comparable results were obtained with Cetuximab conjugated to Alexa Fluor 750 dye (Cetux-Alexa-750). Fluorescence-guided dissection, performed 24 h after injection of Cetuximab conjugated to IRDye 800CW (Cetux-800CW), enabled a real-time delineation of AsPC-1 tumor margins, and small metastases. Odyssey scans revealed that only the vital part of the tumor, but not the necrotic part was stained with Cetux-800CW. NIR fluorescently labeled Cetuximab may be a promising tool that can be applied for fluorescence-guided surgery to visualize tumor margins and metastatic sites in order to allow a precise surgical resection.

The aggressive tumor biology of pancreatic ductal adenocarcinoma (PDAC) together with the asymptomatic early phase of the disease leaves only 10 to 20% of patients as candidates for resection. Within this patient group the so called R1-resection, defined as microscopically positive tumor margins undesirably remaining after surgery, results in a high risk of tumor recurrence of up to 80%.[1–3] This is partially due to the difficulty in the intraoperative assessment of tumor margins, which currently relies only on images taken before the operation, on visual inspection by the surgeons during the resection and on accompanying histological analysis.[4] Fluorescence-guided surgery (FGS), a recent technique introduced in the clinic, in combination with cancer specific fluorescence labels, may improve the precise identification of the local extent of the tumor and the presence of metastasis invisible to the naked eye.

Key words: Cetuximab, near-infrared fluorescence, fluorescence-guided surgery (FGS), IRDye 800CW, clinical translation, pancreatic ductal adenocarcinoma (PDAC), orthotopic pancreatic tumor mouse models

Additional Supporting Information may be found in the online version of this article.

Abbreviations: AEC: 3-amino-9-ethylcarbazole; BSA: bovine serum albumin; EGF: epidermal growth factor; EGFR: epidermal growth factor receptor; ECL: enhanced chemiluminescence substrate; FBS: fetal bovine serum; FDA: Food and Drug Administration; FGS: fluorescence-guided surgery; HE: hematoxylin and eosin; HED: human equivalent dose; HNSCC: head and neck squamous-cell carcinoma; ICG: indocyanine green; i.p.: intraperitoneal; i.v.: intravenous; LT: lifetime; MB: methylene blue; MFI: median fluorescence intensity; NC: normalized counts; NIR: near-infrared; NIRF: near-infrared fluorescence; PBS: phosphate-buffered saline; PDAC: pancreatic ductal adenocarcinoma; PFA: paraformaldehyde; RIPA: radioimmunoprecipitation assay; RSA: sample reducing agent; RT: room temperature; SPECT: single photon emission computed tomography; TPSF: temporal point spread function; 5-ALA: 5-aminolevulinic acid

Grant sponsors: European Commission and FP7-PEOPLE-2011-ITN; **Grant number:** 289648—IonTraC; **Grant sponsor:** H2020-MSCA-RISE; **Grant number:** 644373—PRISAR

DOI: 10.1002/ijc.30277

History: Received 24 Feb 2016; Accepted 23 June 2016; Online 18 July 2016

Correspondence to: Joanna Napp, Department of Molecular Biology of Neuronal Signals, Max-Planck-Institute of Experimental Medicine, Hermann-Rein-Straße 3, D-37075 Göttingen, Germany, Tel.: +49 (0)551-3899-272, E-mail: napp@em.mpg.de or nappjoanna@yahoo.com

What's new?

The combination of cancer-specific fluorescent labels and fluorescence-guided surgery (FGS) is a promising approach to improve the visualization of tumor margins and metastatic sites during surgery to remove cancer. This study shows that precise surgical resection is facilitated significantly by the use of near-infrared fluorescently labeled Cetuximab (Cetux-800CW), a therapeutic antibody targeting the epidermal growth factor receptor. In mice bearing pancreatic ductal adenocarcinomas, Cetux-800CW enabled clear delineation of tumor margins and detection of invasive nodules in the stomach, duodenum, and other organs. Cetux-800CW, through improving the precision of tumor margin assessment, could help reduce the likelihood of recurrence following surgery.

FGS is based on the real time detection of labeled structures emitting NIR fluorescence (NIRF) light in the range between 650 and 950 nm, outside the visible spectrum, and therefore does not change the look of the surgical field.[5] In preclinical settings, NIRF imaging is routinely applied as it is a simple and safe method providing *in vivo* functional information *e.g.* on probe binding and biodistribution, protein expression, enzyme activity, pH or oxygen levels. [6–10] For preclinical research an enormous diversity of fluorescent labels is available, such as Alexa Fluor and Cyanine dyes, but their use in the clinic is still limited due to their possible toxicity.

Up to now, only three NIRF dyes are approved for use in humans, indocyanine green (ICG), methylene blue (MB) and 5-aminolevulinic acid (5-ALA), and are clinically applied for sentinel lymph node mapping in different types of cancers[11–13] and vascular perfusion assessment during or after cancer surgery.[14] Furthermore, they were used for the detection of liver lesions, gliomas and a fibrous tumor of the pancreas, taking advantage of their unspecific accumulation in tumors based on the increased perfusion of tumor vessels.[15–17]

As the lack of clinically available tumor-targeting agents remains one of the principal limitations of FGS, many efforts have been made to conjugate ICG to tumor specific ligands. Unfortunately, once conjugated, ICG often loses/reduces its fluorescence.[18] This problem has persuaded investigators to develop new NIR optical probes with comparable structural and spectral properties as IRDye 800CW or ZW800-1,[19] both currently in the process of clinical translation.

A promising strategy to develop tumor-imaging agents for use in humans involves the conjugation of such new dyes with monoclonal antibodies that are already clinically approved for cancer therapies. Among these is the human/mouse chimeric monoclonal antibody Cetuximab, which targets the epidermal growth factor receptor (EGFR) and we focused our attention on this. EGFR is overexpressed in 70% of pancreatic cancers[20] and in many other human cancers, including head and neck squamous-cell carcinoma (HNSCC), colorectal- and brain cancer.[21] Cetuximab is clinically applied for treatment of patients with *e.g.* colorectal cancer or HNSCC.[22,23] In murine PDAC models, studies have demonstrated the inhibitory effect of Cetuximab on pancreatic tumor growth, although further clinical trials did not show notable improvements in the response rate and survival of the patients.[24] Due to its high affinity for EGFR similar to its natural ligand epidermal growth factor (EGF) ($K_d = 0.38$ nM),[25] NIRF-labeled Cetuximab has been successfully employed for the detection of different tumor xenografts such as breast, tongue or HNSCC by NIRF imaging.[26–28]

The aim of our study was to preclinically evaluate fluorescently labeled Cetuximab as a probe to visualize primary pancreatic tumors and their metastatic spread before and during FGS, for a potential future application in cancer patients. We conjugated Cetuximab with two different preclinical NIRF dyes, Alexa Fluor 647 and Alexa Fluor 750, as well as with a dye that is currently in the process of clinical translation, IRDye 800CW. Orthotopic PDAC xenografts were applied for this study, which exhibit the metastatic cascade typical of human PDAC.[29] Using preclinical fluorescence imaging systems, Optix MX2 and IVIS Spectrum, as well as the Quest Spectrum clinical device for FGS, we show that fluorescently labeled Cetuximab allows the visualization of primary tumors and the metastatic spread in two EGFR-expressing PDAC mouse models, AsPC-1 and MIA PaCa-2, showing promise for future clinical translation in FGS.

Material and Methods

Cell lines and culture conditions

Cell lines were purchased from ATCC (Rockville, MD) and cultivated at 37°C in a humidified atmosphere of 5% CO_2. The human PDAC cells AsPC-1 and BxPC-3 and the human mammary carcinoma cells MDA-MB-468 and MCF7 were grown in RPMI-1640 media (Life Technologies) supplemented with 10% fetal bovine serum (FBS Gold, PAA Laboratories Gold). The human PDAC cells Capan-1 were grown in IMDM medium (Life Technologies), supplemented with 20% FBS, PANC-1 in high-glucose (4.5 g/l) DMEM medium (Life Technologies), supplemented with 10% FBS and MIA PaCa-2 in DMEM/F12 medium (Life Technologies), supplemented with 10% FBS and 2.5% horse serum (Biochrom).

Western-blot analysis

Cells were lysed with radioimmunoprecipitation assay (RIPA) buffer (Sigma Aldrich). 30 μg of proteins, reduced by 50 mM of sample reducing agent (RSA) (Novex), were separated on a 3 to 8% polyacrylamide precast gel (Life Technologies) and

blotted to a nitrocellulose membrane (Amersham Biosciences). The membrane was blocked with 5% bovine serum albumin (BSA, Sigma Aldrich) in 0.05% TBS-Tween 20 for 1 h at room temperature (RT), incubated overnight at 4°C with a rabbit polyclonal anti-EGFR antibody (1 1,000,2232, Cell Signaling) or mouse monoclonal anti-β-Actin antibody (1:1,000, #MAB1501, Merck Millipore), each in TBS-Tween 0.05% and 5% BSA. Blots were incubated with the HRP-conjugated anti-rabbit or anti-mouse antibodies (1:8,000, GE Healthcare Life Sciences) and visualized with enhanced chemiluminescence substrate (ECL, Biological Industries).

Flow cytometry

AsPC-1 and MIA PaCa-2 cells were detached by brief incubation with 0.25% trypsin-EDTA (Life Technologies), followed by neutralization with the corresponding cell culture medium, and were then washed once with phosphate-buffered saline (PBS) and counted. 5×10^5 cells were incubated with Cetuximab (10 μg/ml in PBS, Erbitux, Merck) for 1 h at RT and washed three times with PBS followed by incubation with Protein G coupled to Alexa Fluor 488 (4 μg/ml in PBS, Thermo Fisher Scientific) for 30 min. Fluorescence intensities were measured on a FACSAria cell sorter with FACSDiva software (BD Bioscience). Data were analyzed using FlowJo software 8.8.7 (Tree Star).

Fluorescent probes

Cetuximab was either coupled to Alexa Fluor 647, to Alexa Fluor 750 (Life Technologies; Cetux-Alexa-647 and Cetux-Alexa-750) or to IRDye 800CW (LI-COR Biosciences; Cetux-800CW) resulting in dye-to-protein ratios of 6.7, 4.0 and 0.6, respectively. Human IgG (Jackson ImmunoResearch) was coupled to Alexa Fluor 750 dye (hIgG-Alexa-750) with a dye-to-protein ratio of 5.3. Conjugations were carried out by Squarix Biotechnology (Marl, Germany).

Fluorescence staining of living cells

2×10^5 AsPC-1 or MIA PaCa-2 cells were grown overnight on coverslips in 24-well plates. Afterwards, living cells were incubated for 1 h at 37°C with Cetux-Alexa-647 or Cetux-Alexa-750 (10 μg/ml in medium), washed three times with PBS, fixed with 4% paraformaldehyde (PFA) for 10 min and mounted in Prolong Gold Antifade Reagent with DAPI (Thermo Fisher Scientific).

Animals, tumor cell transplantation and dissection

All animal experiments were performed in accordance with German animal ethics regulations and were approved by the local ethics office of Lower Saxony (license no. 33.9–42502-04–13/1085). Experiments were performed on male athymic nude mice NMRI-*Foxn1*^{nu}, 10 to 20 weeks (Charles River Laboratories). Animals were housed in ventilated cages and allowed food and water *ad libitum*.

1×10^6 AsPC-1 or MIA PaCa-2 cells were resuspended in 20 μl of PBS and transplanted into the head of the pancreas of mice anesthetized by intraperitoneal (i.p.) injection of 15 mg/kg xylazine (Ecuphar) and 75 mg/kg ketamine (Medistar), as previously described.[29] For analgesia, mice received rimadyl (carprofen; 5 mg/kg, Norbrook) i.p. during surgery and metamizole (1.33 mg/ml, Zentiva) in drinking water for 2 days before and for 3 days after surgery. Mice were inspected three times a week for weight loss, general condition, and tumor formation.

Mice were sacrificed by isoflurane (Abbvie) overdose and cervical dislocation. Tumor sizes were measured with a caliper and volumes were calculated using the formula: volume (mm^3) = 0.5 × (length × width × height). Subsequently, numbers and location of macroscopic metastases were observed and counted during dissection.

NIRF imaging and fluorescence-guided autopsy

For *in vitro* fluorescence lifetime (LT) measurement, Cetux-Alexa-647 and hIgG-Alexa-750 were diluted in RPMI-1640 media containing 10% FBS, pipetted on a petri dish and scanned with the Optix MX2 (ART). LT was calculated as previously described.[7]

One week before *in vivo* imaging experiments, mice received chlorophyll-free chow (Scientific Animal Food & Engineering). All *in vivo* analyses were preceded by native scans. AsPC-1 and MIA PaCa-2 tumor bearing mice received intravenously (i.v.) ∼30 and ∼90 days after transplantation, respectively, a single dose of Cetux-Alexa-647 together with hIgG-Alexa-750 (25 μg each in 150 μl of 0.9% NaCl). A single dose of Cetux-Alexa-750 (25 μg in 150 μl of 0.9% NaCl) was injected in AsPC-1 tumor bearing mice ∼30 days after implantation.

Mice were anesthetized with 2% vaporized isofluorane and scanned *in vivo* with Optix MX2 or IVIS Spectrum using the settings shown in Table 1. *In vivo* LTs were calculated from 24 h scans performed with Optix MX2. At 48 h mice were sacrificed, and organs were excised, rinsed with PBS, imaged with Optix MX2 or IVIS Spectrum and fixed with 4% formalin.

Optix 2.02.01 and OptiView 2.01.00 software (ART) were used to acquire and analyze the Optix MX2 data, respectively. Living Image software 4.4 (Perkin Elmer) was used for IVIS-Spectrum image acquisition and analysis.

For fluorescence-guided dissection, AsPC-1 tumor bearing mice received i.v. Cetux-800CW (25 μg in 150 μl of 0.9% NaCl) ∼30 days after transplantation and were sacrificed 24 h later. Dissections were guided with the Quest Spectrum system supported by Artemis Capture Suite 1.1.2 software (Quest Diagnostics) and using settings described in Table 1.

Tissue staining

Fixed tissues were embedded in paraffin and cut in 2 μm thick sections. Sections were deparaffinized, rehydrated and pre-treated at 98°C for 20 min in citrate buffer (pH 6.0, Dako). Hematoxylin and eosin (HE) staining was performed as previously described.[29] For immunofluorescence staining, autofluorescence was blocked with 0.1 M glycin for 10 min at

Table 1. Scan settings used for *in vitro*, *in vivo*, *ex vivo* NIRF imaging, and NIRF microscopy

Optix MX2	**Excitation (nm)**	**Emission (nm)**		
Alexa Fluor 647	635	670 ± 20		
Alexa Fluor 750	730	≥770		
Optix MX2	**Laser power (μW)**	**Integration time (s)**	**Raster (mm)**	
In vivo scans	100	1	1	
Ex vivo/in vitro scans	100	0.5	1.5	
IVIS spectrum	**Excitation (nm)**	**Emission (nm)**		
Alexa Fluor 647	625–660	670–690		
Alexa Fluor 750	730–760	790–810		
IVIS spectrum	**Exposure time**	***f*/stop**	**Binning**	**Field of view (FOV)**
In vivo/*ex vivo* scans	Automatic	2	8	13.3
Quest spectrum	**Excitation (nm)**	**Emission (nm)**		
IRDye 800CW	785	>808		
Fluorescence microscopy	**Excitation (nm)**	**Emission (nm)**		
Alexa Fluor 647	640 ± 15	690 ± 25		
Alexa Fluor 750	708 ± 37.5	809 ± 40.5		
Alexa Fluor 488	470 ± 20	540 ± 25		
DAPI	365 ± 12.5	445 ± 25		

RT and unspecific binding sites were blocked with SEA BLOCK blocking buffer (Thermo Fisher Scientific) for 20 min. Slices were incubated overnight with rabbit-anti-human EGFR antibody (Thermo Fisher Scientific, clone SP9; 1:500), incubated at RT for 1 h with the secondary anti-rabbit antibody-Alexa-Fluor 488 (Life Technologies; 1:400), counterstained with DAPI (Thermo Fisher Scientific; 4 μg/ml) and mounted with Aquatex aqueous mounting medium (Merck). Two washing steps with TRIS buffer were performed between each step. For tissue imaging with Odyssey fluorescence flatbed scanner (LI-COR Biosciences), paraffin sections were deparaffinized, rehydrated and mounted with Aquatex aqueous mounting medium (Merck).

For immunohistochemistry, sections were deparaffinized, rehydrated and pretreated as described earlier. Slides were then incubated for 10 min with 3% H_2O_2 and unspecific binding sites were blocked for 20 min with SEA BLOCK blocking buffer (Thermo Fisher Scientific). Slices were incubated overnight with rabbit-anti-human EGFR antibody (Thermo Fisher Scientific, clone SP9; 1:500) followed by 1 h incubation with N-Histofine Simple Stain Max PO anti-rabbit (Nichirei) and stained with 3-amino-9-ethylcarbazole (AEC). All slices were counterstained with Mayer hematoxylin (Merck) and mounted with Aquatex aqueous mounting medium (Merck). Two washing steps with TRIS buffer were performed between each step.

Fluorescence microscopy and tissue imaging

An Axiovert 200M fluorescence microscope (Carl Zeiss) equipped with a NIR-sensitive ORCA-ER digital camera (Hamamatsu) was used for NIRF microscopy with settings specified in Table 1. HE sections were analyzed with a AxioCamHR camera (Carl Zeiss). Cetux-800CW fluorescence was measured on unstained paraffin sections (2 μm) with the Odyssey fluorescence flatbed scanner (LI-COR Biosciences) using the 800 nm channel (Table 1). Image generation and processing were performed with the software AxioVision Rel.4.6 (Carl Zeiss) and ImageJ,[30] respectively.

Statistical analysis

The significance was analyzed by two-tailed unpaired Student's *t*-test using the program Past.[31] Statistical significance was defined as $p \leq 0.05$.

Results

Pancreatic tumor cells express different levels of EGFR *in vitro*

EGFR expression was assessed by Western Blotting in five human PDAC cell lines: AsPC-1, PANC-1, BxPC-3, MIA PaCa-2 and Capan-1, along with lysates of positive and negative controls, MDA-MB-468 (+) and MCF7 (−) breast cancer cells, respectively. Bands at the expected molecular weight of 170 kDa were recognized (Fig. 1*a*) in all cell lines except Capan-1. A high expression of EGFR was found in AsPC-1 and BxPC-3 cells, as well as moderate and low expression in PANC-1 and MIA PaCa-2 cells, respectively. The anti-β-actin antibody showed equal amount of protein loading in each lane.

Cetuximab binds to EGFR-expressing human AsPC-1 and MIA PaCa-2 cells *in vitro*

To confirm the expression of EGFR on the cell surface, flow cytometry was performed using unlabeled Cetuximab

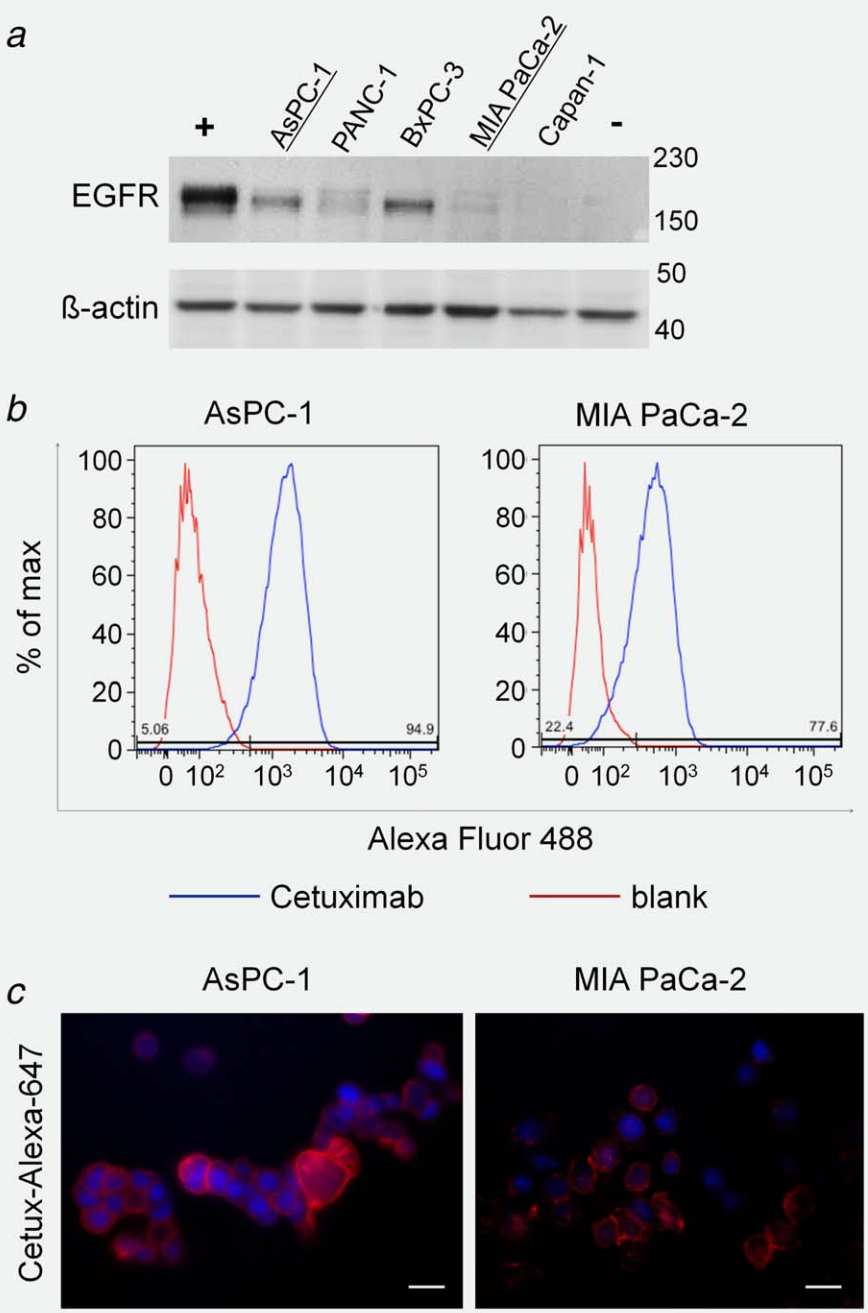

Figure 1. Expression of EGFR in PDAC cells and *in vitro* binding specificity of Cetux-Alexa-647 to AsPC-1 and MIA PaCa-2 PDAC cells. (*a*) Western blot analysis shows high EGFR expression in AsPC-1 and BxPC-3 cells, moderate expression in PANC-1 cells, low expression in MIA PaCa-2 cells, and no expression in Capan-1 cells. MDA-MB-468 and MCF7 cells were used as positive (+) and negative (−) control, respectively. ß-actin was used as loading control. (*b*) Flow cytometry analysis of AsPC-1 and MIA PaCa-2 cells incubated with Cetuximab and detected with Protein G coupled to Alexa Fluor 488 (blue line). Higher EGFR expression levels were observed on AsPC-1 cells (94.9% of EGFR-positive cells with MFI = 1,572) than in MIA PaCa-2 cells (77.6% of EGFR-positive cells with MFI = 564). Red line corresponds to cells incubated without antibody (blank). (*c*) Immunofluorescence staining of living cells revealed strong Cetux-Alexa-647 derived fluorescence on the membrane and within the cytoplasm of AsPC-1 cells and weaker fluorescence mainly on the membrane of MIA PaCa-2 cells (red). The nuclei are counterstained with DAPI (blue). Scale bars represent 20 μm.

revealed by subsequent incubation with protein G coupled to Alexa Fluor 488. As shown in Figure 1b, gating for positive cells based on the unstained cells, revealed that 94.9% of AsPC-1 and 77.6% of MIA PaCa-2 cells were positively stained with Cetuximab with a median fluorescence intensity (MFI) of 1,572 and 564, respectively.

Staining of living AsPC-1 cells with Cetux-Alexa-647 conjugate (Fig. 1*c*) resulted in a strong membrane-bound and

weaker cytoplasmatic staining pattern, indicating partial internalization of the conjugate. In contrast, weaker Cetux-Alexa-647 membrane staining was detected on the MIA PaCa-2 cells. Immunofluorescence analysis of Cetux-Alexa-750 incubated with AsPC-1 cells *in vitro* revealed a similar pattern of membrane and cytosolic staining as seen for Cetux-Alexa-647 (data not shown).

Cetux-Alexa-647 specifically targets PDAC *in vivo*

To test if Cetux-Alexa-647 could serve as an imaging probe to visualize pancreatic tumor spread *in vivo*, we validated the probe in nude mice bearing orthotopic AsPC-1 and MIA PaCa-2 tumors by *in vivo* NIRF imaging.

Mice orthotopically transplanted with AsPC-1 cells showed typical PDAC symptoms within 4 to 5 weeks after transplantation, in particular weight loss of >20% of the initial weight that lasted more than 2 days. For ethical reasons these symptoms were defined by us as criteria for experiment termination and AsPC-1 tumor bearing mice had to be sacrificed. At this time point, AsPC-1 tumors ($n = 6$; Supporting Information Fig. 1a) reached volumes of 96 ± 27 mm^3 and showed invasion into the stomach and duodenum, and massive tumor spread to different sites and organs adjacent to the pancreas such as the left liver lobe, spleen or mesentery (Supporting Information Figs. 1b–1d). Moreover, AsPC-1 tumor nodules were found at the site of surgical incision (Supporting Information Fig. 1e) where a large tumor mass occasionally developed.

Orthotopically transplanted MIA PaCa-2 mice developed symptoms much later, within 12 to 14 weeks after transplantation. At this time point, primary tumors (Supporting Information Fig. 1f) reached volumes of 600 ± 298 mm^3 ($n = 6$), invaded into the stomach and duodenum and occasionally infiltrated the bile duct (Supporting Information Fig. 1g), causing jaundice (Supporting Information Fig. 1h).

To assess the EGFR expression level in AsPC-1 and MIA PaCa-2 primary tumors, we performed staining of human EGFR on tumor sections. Supporting Information Figures 1i–1m illustrates that the two tumor models show different EGFR expression patterns within the tumor tissue. While AsPC-1 tumors show homogenous strong EGFR staining (Supporting Information Figs. 1i and 1j), heterogeneous expression was found in MIA PaCa-2 tumors (Supporting Information Figs. 1k–1m). Weak staining was observed in different areas of the primary tumor mass (Supporting Information Fig. 1l) whereas tumor cells invading the stomach and duodenum showed strong EGFR staining (Supporting Information Fig. 1m). Large and central necrotic areas were present in both, AsPC-1 and MIA PaCa-2 primary tumors (arrow; Supporting Information Figs. 1i and 1k).

Due to the different growth of the tumors, AsPC-1 ($n = 10$) and MIA PaCa-2 ($n = 7$) tumor bearing mice, either ~30 or ~90 days after transplantation, respectively, were injected with Cetux-Alexa-647 alone (25 μg; data not shown) or in combination with the control probe hIgG-Alexa-750 (25 μg each). Binding and distribution of both probes were monitored simultaneously at distinct time points up to 48 h using the Optix MX2 (Fig. 2) and IVIS Spectrum (data not shown).

As shown in Figure 2*a*, Cetux-Alexa-647 derived fluorescence in AsPC-1 mice (upper panel; left) was diffusely distributed over the scanned area (white rectangle). This is presumably due to the overlap of signals derived from the probe that accumulated within the primary tumor and the tumor mass grown at the surgical scar as well as the tumor spread into neighboring organs. In the MIA PaCa-2 tumor bearing mice (lower panel; left), Cetux-Alexa-647 derived fluorescence was more localized over the center of the upper abdomen where the primary pancreatic tumors developed. This is in agreement with our observation that MIA PaCa-2 tumors show a lower metastatic potential than AsPC-1 tumors. By contrast, the control hIgG-Alexa-750 probe did not localize to the tumor but showed fluorescence only over the liver in both PDAC models (right panels). In both PDAC models, Cetux-Alexa-647 fluorescence intensities reached their maximum intensities at 24 h after probe injection (Fig. 2*b*), as was the case for the control probe. The same results were obtained with the IVIS Spectrum (data not shown). As shown in Figure 2*b*, quantification of the average fluorescence intensities of Cetux-Alexa-647 over the tumor areas confirmed a significantly higher increase of fluorescence intensities in both, AsPC-1 and in MIA PaCa-2 mice at 24 h and 48 h when compared to values of the prescans.

To confirm the specificity of the fluorescence signals of Cetux-Alexa-647 and hIgG-Alexa-750 detected *in vivo* over the areas of tumor and liver, we compared *in vitro* fluorescence LTs of the conjugates with the fluorescence LTs obtained from the *in vivo* scans performed 24 h after injection of the probe. *In vitro* scans of Cetux-Alexa-647 (left) and hIgG-Alexa-750 (right) revealed LTs of 1.34 ns and 0.59 ns, respectively (Fig. 3*a*). Comparable fluorescence LTs were measured *in vivo* (Fig. 3*b*). Cetux-Alexa-647 (Fig. 3*b*; left and middle) showed *in vivo* LTs of 1.37 ± 0.05 ns at the tumor site in the AsPC-1 and 1.47 ± 0.02 ns in the MIA PaCa-2 mouse model, whereas hIgG-Alexa-750 scans (Fig. 3*b*; right and middle) revealed LTs of 0.73 ± 0.02 ns and 0.71 ± 0.03 ns over the liver in the AsPC-1 and MIA PaCa-2 mouse models, respectively. These results confirm that the signals obtained *in vivo* are specifically derived from the injected NIRF probes.

To exclude any influence of the dye on the distribution of the antibody, Cetuximab was labeled with Alexa Fluor 750 dye (Cetux-Alexa-750). AsPC-1 tumor bearing mice were injected with a single dose of Cetux-Alexa-750 and scanned with the IVIS-Spectrum system (25 μg; $n = 2$). Similar to Cetux-Alexa-647, injection of Cetux-Alexa-750 resulted in a specific accumulation at the primary tumor *in vivo* showing a peak of fluorescence intensity over the tumor area at 24 h (data not shown). Application of Cetux-Alexa-750 also

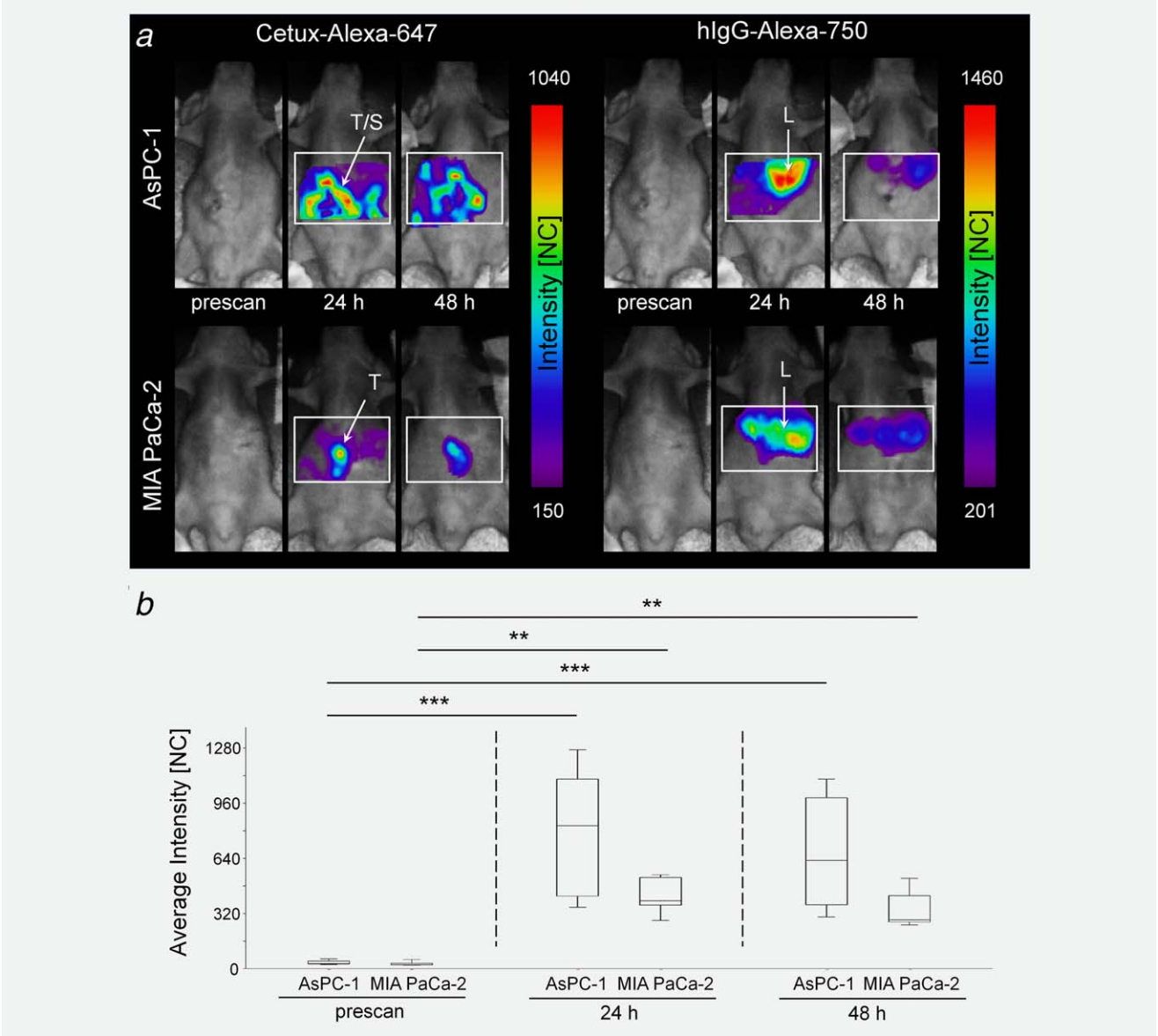

Figure 2. *In vivo* binding of Cetux-Alexa-647 to AsPC-1 and MIA PaCa-2 primary tumors. (*a*) Representative *in vivo* Optix MX2 scans of the upper abdominal area (white rectangle) before, 24 h and 48 h after co-injection of Cetux-Alexa-647 (left) and hIgG-Alexa-740 (right), 25 μg each, in AsPC-1 (upper panel, $n = 10$) and MIA PaCa-2 (lower panel, $n = 7$) tumor bearing mice. Cetux-Alexa-647, but not the control hIgG-Alexa-750, was detected over the AsPC-1 and MIA PaCa-2 primary pancreatic tumors (T), as well as over the tumor mass developed at the site of surgical incision (T/S) in the AsPC-1 model. Fluorescence intensities are displayed in normalized counts (NC). (*b*) Box plot showing significantly higher average fluorescence intensities (NC) measured over the tumor areas at 24 h and at 48 h (***$p < 0.001$ and **$p < 0.01$) than in prescans of both, AsPC-1 and MIA PaCa-2 tumor bearing mice.

resulted in a minor fluorescence signal over the liver (data not shown).

Cetux-Alexa-647 binds to PDAC primary tumor and metastases *in vivo*

To analyze the distribution of Cetux-Alexa-647 in more detail, mice were sacrificed 48 h after injection of the NIRF probes. Primary tumor, tumor mass grown at the site of surgical incision as well as spleen, lung, liver, kidney, mesentery, lymph nodes and diaphragm were excised (Fig. 4*a*, middle panel) and scanned *ex vivo* (Fig. 4*a*, left and right panel). In AsPC-1 tumor-bearing mice, not only the primary tumor (white circle) and tumor mass at the site of surgical incision, but also small metastatic lesions at the diaphragm, the left liver lobe and the mesentery showed a strong accumulation of Cetux-Alexa-647 (left). In contrast, in the MIA PaCa-2 tumor bearing mouse, which did not develop any metastases, no Cetux-Alexa-647 derived fluorescence signals could be detected besides the primary tumor (white circle). In accordance, no hIgG-Alexa-750 derived fluorescence was visible

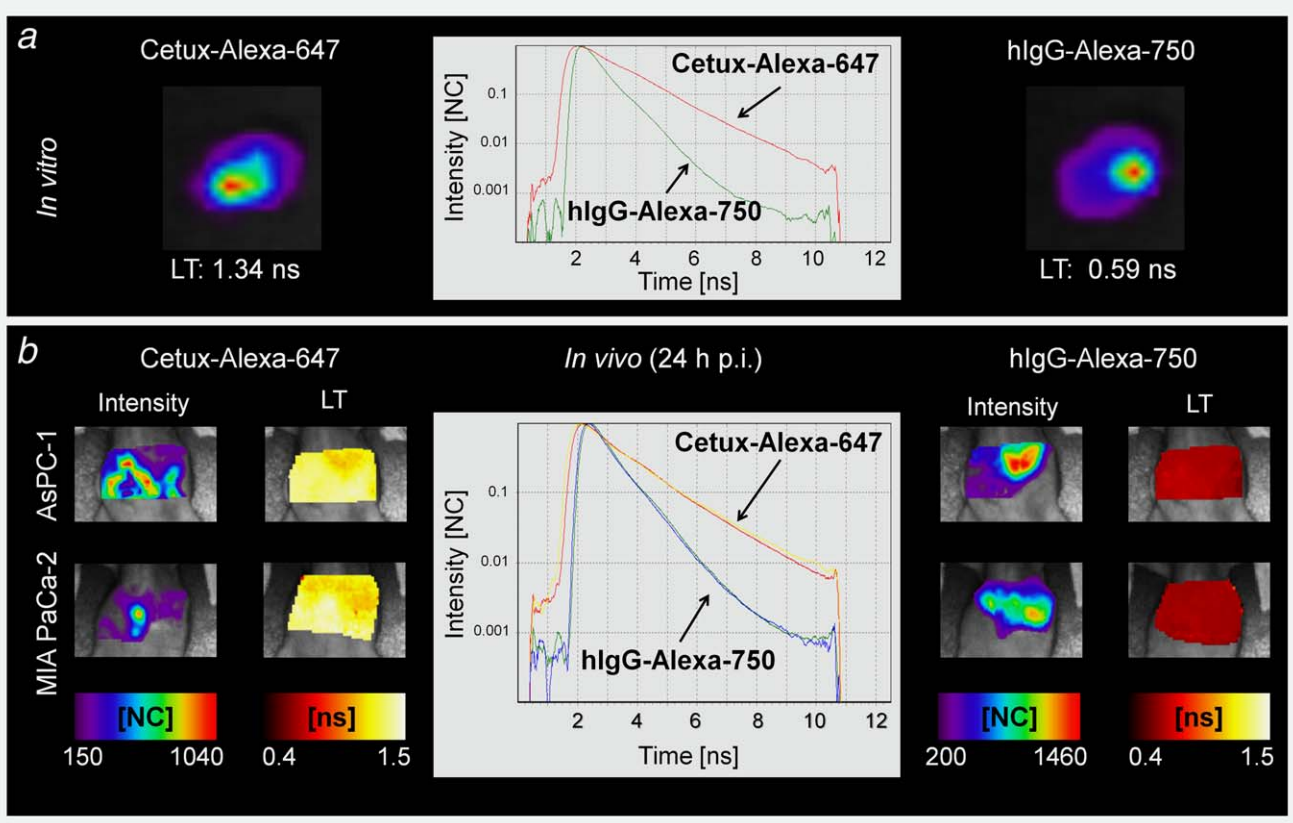

Figure 3. *In vitro* and *in vivo* fluorescence LTs of Cetux-Alexa-647 and hIgG-Alexa-750. (*a*) Representative *in vitro* scans of the Cetux-Alexa-647 (left) and hIgG-Alexa-750 (right) probes performed with the Optix MX2. The middle panel shows the corresponding representative temporal point spread functions (TPSFs). The monoexponential decay of each curve was used to calculate the fluorescence LT of both, the EGFR targeting probe Cetux-Alexa-647 (1.34 ns) and the control probe hIgG-Alexa-750 (0.59 ns). (*b*) Representative *in vivo* intensity scans of AsPC-1 (left) and MIA PaCa-2 (right) tumor bearing mice shown in Figure 2*a*, with corresponding LT maps as well as representative TPSFs (middle panel), demonstrating that *in vivo* fluorescence LTs over the tumors (for Cetux-Alexa-647) and the liver (for hIgG-Alexa-750) are comparable to the *in vitro* lifetimes of each probe. TPSFs are graphed as fluorescence intensity (NC) *versus* time (ns).

over the MIA PaCa-2 or the AsPC-1 tumor area, nor at metastatic sites, but the signals were clearly localized at the liver.

Quantification of the *ex vivo* average fluorescence signals intensities revealed that AsPC-1 tumors displayed significantly higher ($p = 0.04$) Cetux-Alexa-647 fluorescence in comparison to the data obtained in MIA PaCa-2 tumors (Fig. 4*b*, left panel). Only negligible average fluorescence values were measured on hIgG-Alexa-750 scans over tumor areas of both tumor models (Fig. 4*b*, right panel).

Ex vivo analysis of the Cetux-Alexa-750 distribution in AsPC-1 tumor bearing mice 48 h after i.v. injection, confirmed that Cetux-Alexa-750 also accumulated at the primary tumor and metastatic sites (data not shown). Low Cetux-Alexa-750 derived fluorescence was also detected over the liver.

Binding of the i.v. injected Cetux-Alexa-647 to tumor cells was furthermore confirmed by NIRF microscopy of tumor tissue sections. To visualize tumor cells, slices were stained with an anti-human-EGFR antibody targeting a different epitope of the receptor than Cetuximab and detected with an Alexa Fluor 488-labeled secondary antibody. As shown in Figure 4*c*, the *in vivo* administered Cetux-Alexa-647 (red) bound only to EGFR-expressing AsPC-1 and MIA PaCa-2 tumor cells (green). Note, that some AsPC-1 and MIA PaCa-2 cells showed only a green staining (yellow arrows), suggesting that the Cetux-Alexa-647 conjugate did not bind to all EGFR expressing tumor cells within the primary tumor. Signals derived from Cetux-Alexa-647 were found within the entire tumor tissue except in the necrotic area (data not shown). No Cetux-Alexa-647 fluorescence was detected in the healthy pancreatic tissue, stomach and duodenum (data not shown).

As expected, hIgG-Alexa-750 derived fluorescence was not detected within the primary tumor sections.

Similar to Cetux-Alexa-647, NIRF microscopy confirmed binding of the i.v. injected Cetux-Alexa-750 to the majority, but not all, EGFR-expressing AsPC-1 cells of the primary tumors (data not shown).

Cetux-800CW as a tool for fluorescence-guided surgery

To evaluate Cetuximab as a tool for FGS, the antibody was conjugated to the NIRF dye IRDye 800CW (Cetux-800CW) and employed for fluorescence-guided dissection of AsPC-1

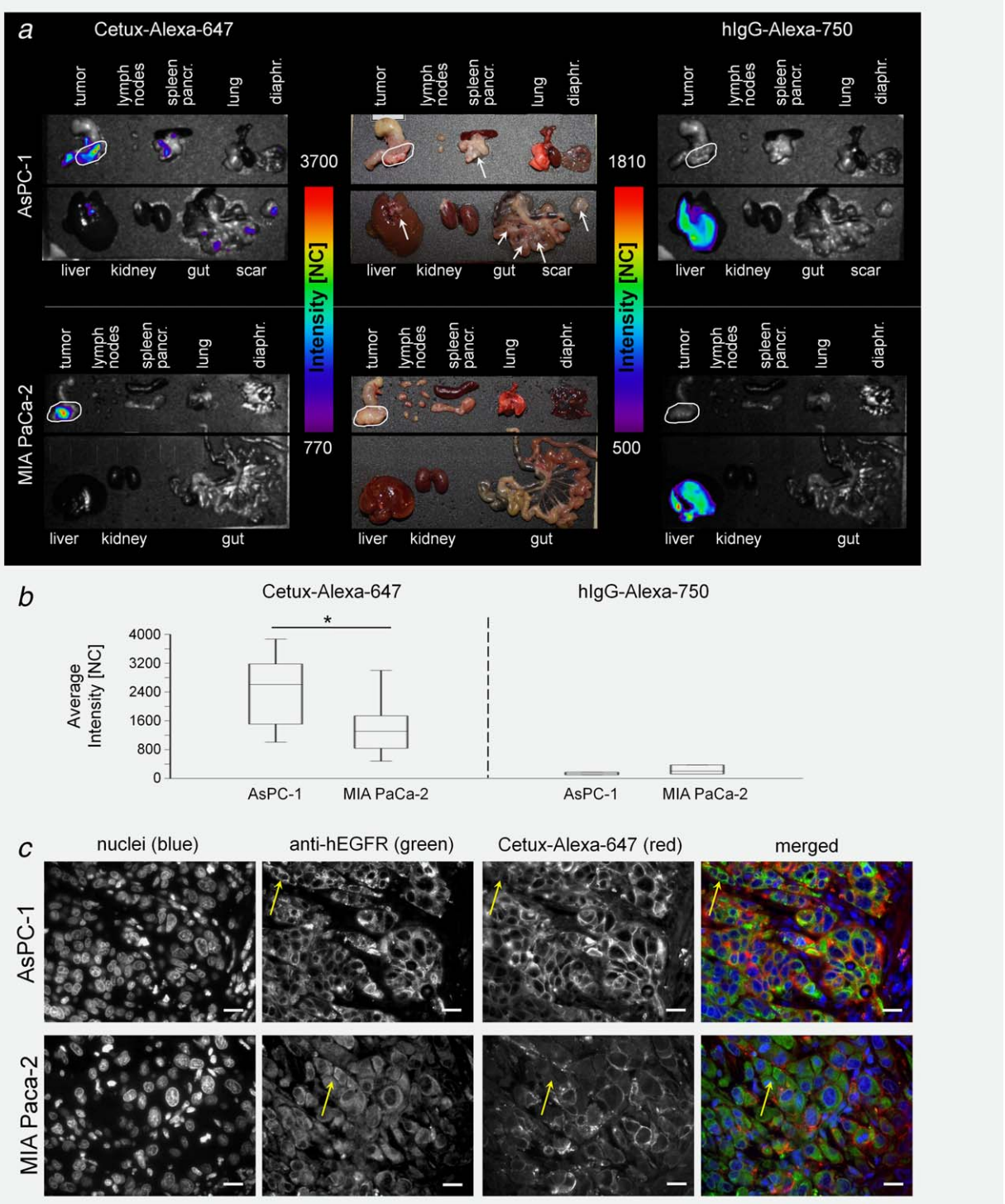

Figure 4. Analysis of biodistribution and binding of Cetux-Alexa-647 by *ex vivo* NIRF imaging and fluorescence microscopy. (*a*) Representative *ex vivo* NIRF scans of Cetux-Alexa-647 (left) and hIgG-Alexa-750 (right) of the excised tumor and organs of AsPC-1 (upper panel) and MIA PaCa-2 (lower panel) tumor bearing mice as well as the corresponding photographs (middle). Cetux-Alexa-647 derived fluorescence was detected over both, AsPC-1 and MIA PaCa-2 primary tumors (white circles) as well as in the AsPC-1 model over metastases in the mesentery, pancreas and in the left liver lobe (arrows). The control hIgG-Alexa-750 was not visible over the tumor area, but accumulated in the liver. (*b*) Box plots of average *ex vivo* fluorescence intensities (NC) of Cetux-Alexa-647 and hIgG-Alexa-750 quantified over the explanted tumors (*$p = 0.04$) are shown. (*c*) NIRF microscopy of AsPC-1 and MIA PaCa-2 primary tumors excised 48 h after i.v. injection of probes and co-stained with an anti-human-EGFR antibody. Counter stain of cell nuclei, stain with anti-hEGFR and Cetux-Alexa-647 derived signals are illustrated, followed by merged images confirmed binding of the *in vivo* applied Cetux-Alexa-647 (red) to the membrane of EGFR-positive tumor cells (green), although not to all (yellow arrows). Nuclei are counterstained with DAPI (in blue). Scale bars represent 20 μm.

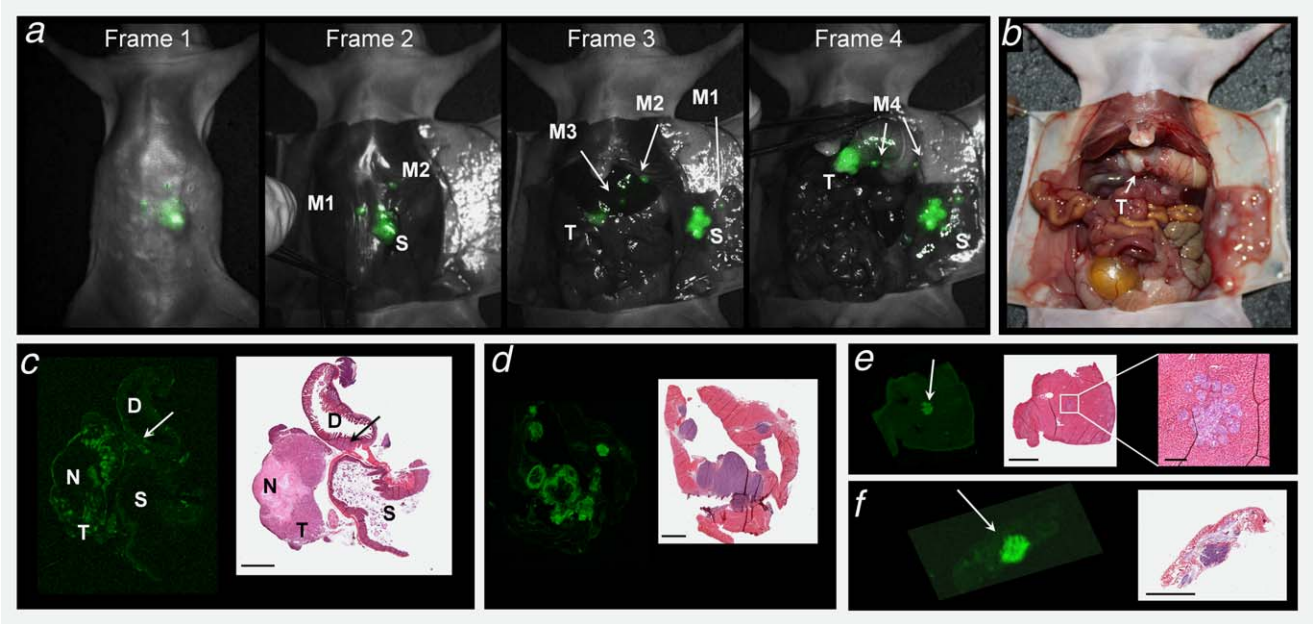

Figure 5. Cetux-800CW as a tool for fluorescence-guided surgery. (*a*) Representative movie-frames (Frame 1–4) recorded with the Quest Spectrum imaging system during fluorescence-guided dissection of AsPC-1 tumor bearing mouse ($n = 5$) 24 h after injection of 25 μg of Cetux-800CW, showing accumulation of the probe (green) within the primary tumor (T), the tumor mass at the surgical incision (S), and small metastases (M1-4). (*b*) Corresponding photograph of the same mouse with opened abdomen, showing tumor lesions that are barely visible without fluorescence guidance. (*c*) Odyssey scan of a representative primary AsPC-1 tumor (T) embedded together with adjacent stomach (S) and duodenum (D) (left) and corresponding HE staining (right). Cetux-800CW derived fluorescence (green) is observed at the vital part of the primary tumor and at the site of tumor invasion (arrow) into the stomach (S) and duodenum (D), but not at the necrotic area (N). (*d–f*) Odyssey scans and HE staining of tissue sections confirming the presence of Cetux-800CW derived fluorescence (*d*) at the tumor mass that developed at the surgical incision and at two small metastases (~1 mm) developed (*e*) at the liver and (*f*) at the costal arch. All the metastatic lesions were also detected beforehand during FGS in (*a*). Scale bars represent 2,000 μm. Scale bar for inset of (*e*) is 200 μm.

xenografts ($n = 5$). Mice were sacrificed 24 h after i.v. injection of 25 μg of Cetux-800CW and dissection was guided and monitored in real-time using the Quest Spectrum clinical system for FGS. Selected frames of a representative movie made during the progressive steps of the dissection are shown in Figure 5*a*. The first two frames show a mouse with intact skin and the peritoneum immediately after sacrifice and exposure to the camera. Three highly fluorescent areas are visible over the upper abdomen: the tumor mass that developed at the surgical scar (S) and two small fluorescent lesions (M1 and M2) that may correlate to metastatic sites. Frame 3 shows the clear delineation of the primary tumor (T) partially covered by the liver at this stage of dissection. The tumor mass that developed at the surgical scar (S) is also visible after opening the peritoneum. Tumor lesions, such as M1 (at the peritoneum) and M2 (at the costal arch) and a further small metastasis at the left liver lobe (M3) were detected at this stage by Quest Spectrum. Frame 4 shows the entire tumor (T) that was exposed to the camera enabling its fluorescence-guided resection. Furthermore, multiple tumor nodules were detected along the stomach (M4), which were barely visible with the naked eye (Fig. 5*b*).

Paraffin sections of the resected primary tumors were scanned with the Odyssey Imager (Fig. 5*c*; left) and the location of the fluorescence was compared to results of HE staining (right). Only the vital part of the primary tumor was stained with the i.v. injected Cetux-800CW (green), whereas the necrotic part in the tumor center (N), confirmed by HE staining (right panel; N), did not show any Cetux-800CW derived fluorescence. Tumor cells invading the stomach and the duodenum (arrow) are also clearly visible. Cetux-800CW derived fluorescence was found in particular at the tumor mass which had developed at the scar (Fig. 5*d*) and at two small (~1 mm) metastases: in the liver lobe (Fig. 5*e*) and at the costal arch (Fig. 1*f*), whereas the healthy tissue (duodenum and stomach epithelium, liver and peritoneum) did not present any Cetux-800CW signal.

Discussion

To our knowledge, these results are the first to show the potential of the clinically approved monoclonal therapeutic antibody Cetuximab, labeled with NIRF dyes, to detect pancreatic tumors and their metastatic spread in mice using non-invasive *in vivo* NIRF imaging and *ex vivo* fluorescence-guided dissection.

We demonstrated by *in vivo* optical imaging that Cetux-Alexa-647, but not the control human hIgG-Alexa-750, accumulates at the AsPC-1 and MIA PaCa-2 tumor sites only, with a maximum fluorescence 24 h after injection. By *ex vivo* imaging, we detected fluorescence signals at metastatic lesions

as small as 1 mm in the highly metastatic AsPC-1 model, whereas no fluorescence signals were observed in the peritoneal organs of MIA PaCa-2 model, confirming the different metastatic behavior of the two PDAC xenografts. No comparable fluorescence was observed in other organs such as liver or kidney, in contrast to previous optical imaging studies where unspecific accumulation was often found due to the metabolism of the used probes.[32–34]

We confirmed the specificity of Cetux-Alexa-647 and hIgG-Alexa-750 derived fluorescence by comparing their fluorescence LTs measured *in vivo* at 24 h over the tumor and the liver, with the LTs of the probes dissolved in medium. Slightly higher LT values were measured *in vivo* which is in agreement with our previous observations, showing that LT of fluorescently labeled antibodies can be slightly influenced by *in vivo* conditions, such as the presence of serum proteins in the blood.[7]

Additionally, any interference of the dye with the biodistribution of Cetuximab was excluded by conjugating it with a longer wavelength NIRF dye, Alexa Fluor 750, used in our initial experiments for labeling the control human IgG. Analogous to results obtained with Cetux-Alexa-647, Cetux-Alexa-750 derived fluorescence was detected specifically at the AsPC-1 primary tumor and metastatic sites. The low Cetux-Alexa-750 derived fluorescence observed over the liver, which was not detected in the *in vivo* and *ex vivo* scans of mice that received Cetux-Alexa-647, can be explained by the improved tissue penetration of the longer wavelength light (~750 nm). However, the low liver fluorescence did not affect the detection of primary tumors and liver metastases, which had a much higher intensity and were clearly visible with all used fluorescent labels.

Previous studies which used radiolabeled Cetuximab in combination with highly sensitive technologies, such as single photon emission computed tomography (SPECT) have shown much higher liver signals.[35,36] This is clearly a significant limitation of SPECT in combination with therapeutic antibodies for the detection of tumors that develop next to the liver. We believe that our fluorescence approach, in addition to being a safe procedure, benefits from both, a very high tumor signal and a comparably low liver background, thus effectively allowing *in vivo* detection of PDAC as well as metastases within the liver of mice.

By quantifying the *ex vivo* average fluorescence intensities we showed that uptake of Cetux-Alexa-647 by high EGFR-expressing AsPC-1 primary tumors was significantly higher than by low EGFR-expressing MIA PaCa-2 primary tumors. However, the difference in the *ex vivo* fluorescence intensity between the two tumor types was lower than the one observed *in vitro* by FACS analysis, or when comparing the intensity of the Western blot bands. This can be in part explained by the heterogeneous EGFR expression observed only throughout the MIA PaCa-2, but not AsPC-1 primary tumor sections, with some areas showing low EGFR expression and others characterized by a relatively high expression of the EGFR, especially within the invasion front in the stomach and duodenum. A similar discrepancy between expression levels and *in vivo* fluorescence intensity was observed by others and has been explained by different morphological features of the cells[37] or by receptor-mediated internalization of the antibody.[27]

Because the biodistribution of Cetux-Alexa-647 revealed a maximum peak of fluorescence intensity over the PDAC tumors 1 day after i.v. injection, fluorescence-guided dissection was performed 24 h after application of Cetux-800CW, providing enough time for the NIRF probe to circulate and bind to the tumor tissue. This is in accordance with studies performed in non-human primates and in humans, demonstrating that serum half-life of Cetux-800CW varies between 1.2 and 2.5 days, depending on dose and species.[38,39]

The amount of i.v. injected NIRF labeled Cetuximab used for this study (25 μg per mouse corresponding to ~0.8 mg/kg of body weight) is comparable to the human equivalent dose (HED) of 0.06 mg/kg of body weight or to 29.6 mg/m^2 based on body surface area.[40] This is in agreement with the only clinical study employing Cetux-800CW for the detection of squamous-cell carcinomas, showing that the maximum tumor to background ratio was obtained at the dose of 25 mg/m^2.[38]

Using the clinically approved Quest Spectrum system in combination with Cetux-800CW, a successful resection of the primary tumor was carried out during *ex vivo* dissection of AsPC-1 xenografts and identification of multiple metastatic nodules as small as 1 mm was possible. High tumor signals were detected even through the intact skin and despite the inhomogeneous lighting conditions of the open camera set up which result in a lower detection efficacy compared to the preclinical systems such as Optix MX2 and IVIS Spectrum.

By fluorescence microscopy of both, AsPC-1 and MIA PaCa-2 tumor tissues, we showed that not all EGFR-expressing tumor cells had bound detectable levels of the i.v. injected Cetux-Alexa-647 and Cetux-Alexa-750. This may be due to the poor vascularization of the pancreatic tumors, which may simply prevent the sufficient diffusion of the Cetuximab throughout the tumor tissue. Moreover, the high affinity of Cetuximab together with its large size may also influence its extravasation and diffusion into the less vascularized regions.[41] Nevertheless, the inhomogeneous binding of the injected probe to the tumor does not seem to have a significant impact on the detection capacity, as we were able to detect metastases as small as 1 mm in the highly metastatic AsPC-1 mouse model.

Furthermore, using NIRF microscopy we did not detect any false positives. Neither the pancreatic acini nor the epithelium of the stomach and the duodenum surrounding the PDAC tumor were stained with Cetux-Alexa-647, confirming the specificity of the conjugate to only recognize the human EGFR on tumor cells.

Odyssey scans of tumor tissue slices confirmed the specificity of Cetux-800CW, by demonstrating that it binds

exclusively to the AsPC-1 tumor cells and does not accumulate in the necrotic areas of the tumors, also in line with recently described results for clinical samples.[38] The presence of necrosis in the tumor does not impede the visualization of the surgical margins, since the vital tumor cells targeted by the fluorescently labeled Cetuximab are mainly located at the periphery of the tumor.

To date, there has only been one preclinical study describing the application of the clinical Quest Spectrum system, which showed the visualization of tongue tumors and of sentinel lymph nodes in mice.[42] The same authors have also described a clinical trial, using the Quest Spectrum for the detection of human colorectal liver metastases that were located near or at the liver surface, 24 h after injection of ICG. Two other FDA-approved intraoperative fluorescence imaging systems, SPY and FLARE, were used in preclinical studies in combination with different therapeutic monoclonal antibodies labeled with IRDye 800CW, *e.g.* for the surgical resection of breast cancer,[26] HNSCC,[27] and for the visualization of pancreatic xenografts using a CEA-targeting single-chain antibody fragment labeled with IRDye 800CW.[43] Moreover, Metildi *et al.*,[44,45] reported different laparoscopic preclinical approaches of pancreatic surgery in combination with anti-CEA antibody labeled with Alexa Fluor 488 dye showing clear benefits on survival rates. Although this approach was very promising, the clinical translation will be difficult, due to the possible toxicity of preclinical Alexa Fluor dyes and because the antibodies used are not clinically approved.

Clinical approval of a probe requires that each component must be examined individually for its toxicity. The more multi-componential the probe, the more difficult will be its approval. The best option is therefore to combine components that are already clinically approved, such as Cetuximab and the NIRF dye IRDye 800CW, which is currently in the process for clinical translation. It has to be noted that the administration of Cetuximab in patients has been correlated with hypersensitivity.[46] While the immunogenicity of the single components has not been considered in this study, this issue should be carefully analyzed in the future by using immunocompetent mice.

Our NIRF approach, although very promising in addressing the visualization of EGFR positive PDAC tumors and metastatic spread, is not without limitations. First of all, micro metastases and circulating tumor cells cannot be detected. Moreover, as not all pancreatic tumors express EGFR and because clinical tumors are in general heterogeneous and the expression patterns differ between the individual patients, the clinical application of Cetux-800CW alone for FGS may not be sufficient to visualize all tumor cells. Therefore, studies for tumor targeting should follow, which evaluate different monoclonal antibodies directed against known tumor markers of PDAC,[47] with the aim towards the use of a probe "cocktail" to maximize the number of labeled tumor cells in PDAC patients.

Conclusion

This study presents fundamental evidence that intravenously applied Cetuximab-dye conjugates can be used as specific contrast agents for the detection of primary tumor burden and metastatic nodules in PDAC tumor bearing mice. In addition, NIRF labeled Cetuximab may be a useful tool for fluorescence-guided cancer surgery leading to significant improvements in the resection of tumors and providing a realistic solution to address positive margin rates.

Acknowledgements

Authors thank Andrea Markus for proof-reading the manuscript, and Bärbel Heidrich, Roswitha Streich, Sarah Garbode, Sabine Wolfgramm, Bettina Jeep and Hanna Puchala for excellent technical assistance.

References

1. Fatima J, Schnelldorfer T, Barton J, et al. Pancreatoduodenectomy for ductal adenocarcinoma: implications of positive margin on survival. *Arch Surg* 2010;145:167–72.
2. Konstantinidis IT, Warshaw AL, Allen JN, et al. Pancreatic ductal adenocarcinoma: is there a survival difference for R1 resections versus locally advanced unresectable tumors? What is a "true" R0 resection? *Ann Surg* 2013;257:731–6.
3. Rau BM, Moritz K, Schuschan S, et al. R1 resection in pancreatic cancer has significant impact on long-term outcome in standardized pathology modified for routine use. *Surgery* 2012;152: S103–11.
4. Pleijhuis RG, Graafland M, de Vries J, et al. Obtaining adequate surgical margins in breast-conserving therapy for patients with early-stage breast cancer: current modalities and future directions. *Ann Surg Oncol* 2009;16:2717–30.
5. Frangioni JV. New technologies for human cancer imaging. *J Clin Oncol* 2008;26:4012–21.
6. Wang L, Fan Z, Zhang J, et al. Evaluating tumor metastatic potential by imaging intratumoral acidosis via pH-activatable near-infrared fluorescent probe. *Int J Cancer* 2015;136:E107–E116.
7. Napp J, Dullin C, Muller F, et al. Time-domain in vivo near infrared fluorescence imaging for evaluation of matriptase as a potential target for the development of novel, inhibitor-based tumor therapies. *Int J Cancer* 2010;127: 1958–74.
8. Mathejczyk JE, Pauli J, Dullin C, et al. High-sensitivity detection of breast tumors in vivo by use of a pH-sensitive near-infrared fluorescence probe. *J Biomed Opt* 2012;17:076028.
9. Markus MA, Dullin C, Mitkovski M, et al. Non-invasive optical imaging of eosinophilia during the course of an experimental allergic airways disease model and in response to therapy. *PLoS One* 2014;9:e90017.
10. Napp J, Behnke T, Fischer L, et al. Targeted luminescent near-infrared polymer-nanoprobes for in vivo imaging of tumor hypoxia. *Anal Chem* 2011;83:9039–46.
11. Cahill RA, Anderson M, Wang LM, et al. Near-infrared (NIR) laparoscopy for intraoperative lymphatic road-mapping and sentinel node identification during definitive surgical resection of early-stage colorectal neoplasia. *Surg Endosc* 2012; 26:197–204.
12. Tajima Y, Yamazaki K, Masuda Y, et al. Sentinel node mapping guided by indocyanine green fluorescence imaging in gastric cancer. *Ann Surg* 2009;249:58–62.
13. van der Vorst JR, Schaafsma BE, Verbeek FP, et al. Dose optimization for near-infrared fluorescence sentinel lymph node mapping in patients with melanoma. *Br J Dermatol* 2013;168: 93–8.
14. Newman MI, Samson MC. The application of laser-assisted indocyanine green fluorescent dye angiography in microsurgical breast reconstruction. *J Reconstr Microsurg* 2009;25:21–6.
15. Ishizawa T, Fukushima N, Shibahara J, et al. Real-time identification of liver cancers by using indocyanine green fluorescent imaging. *Cancer* 2009;115:2491–504.
16. Stummer W, Pichlmeier U, Meinel T, et al. Fluorescence-guided surgery with 5-aminolevulinic

acid for resection of malignant glioma: a randomised controlled multicentre phase III trial. *Lancet Oncol* 2006;7:392–401.
17. van der Vorst JR, Vahrmeijer AL, Hutteman M, et al. Near-infrared fluorescence imaging of a solitary fibrous tumor of the pancreas using methylene blue. *World J Gastrointest Surg* 2012; 4:180–4.
18. Kosaka N, Ogawa M, Choyke PL, et al. Clinical implications of near-infrared fluorescence imaging in cancer. *Future Oncol* 2009;5:1501–11.
19. Vahrmeijer AL, Hutteman M, van der Vorst JR, et al. Image-guided cancer surgery using near-infrared fluorescence. *Nat Rev Clin Oncol* 2013; 10:507–18.
20. Tobita K, Kijima H, Dowaki S, et al. Epidermal growth factor receptor expression in human pancreatic cancer: Significance for liver metastasis. *Int J Mol Med* 2003;11:305–9.
21. Shaib W, Mahajan R, El-Rayes B. Markers of resistance to anti-EGFR therapy in colorectal cancer. *J Gastrointest Oncol* 2013;4:308–18.
22. Fung C, Grandis JR. Emerging drugs to treat squamous cell carcinomas of the head and neck. *Expert Opin Emerg Drugs* 2010;15:355–73.
23. Schuch G, Kobold S, Bokemeyer C. Evolving role of cetuximab in the treatment of colorectal cancer. *Cancer Manage Res* 2009;1:79–88.
24. Luedke E, Jaime-Ramirez AC, Bhave N, III, et al. Monoclonal antibody therapy of pancreatic cancer with cetuximab: potential for immune modulation. *J Immunother* 2012;35:367–73.
25. Kim GP, Grothey A. Targeting colorectal cancer with human anti-EGFR monoclonocal antibodies: focus on panitumumab. *Biologics* 2008;2:223–8.
26. Korb ML, Hartman YE, Kovar J, et al. Use of monoclonal antibody-IRDye800CW bioconjugates in the resection of breast cancer. *J Surg Res* 2014; 188:119–28.
27. Day KE, Sweeny L, Kulbersh B, et al. Preclinical comparison of near-infrared-labeled cetuximab and panitumumab for optical imaging of head and neck squamous cell carcinoma. *Mol Imaging Biol* 2013;15:722–9.
28. Withrow KP, Gleysteen JP, Safavy A, et al. Assessment of indocyanine green-labeled cetuximab to detect xenografted head and neck cancer cell lines. *Otolaryngol Head Neck Surg* 2007;137: 729–34.
29. Alves F, Contag S, Missbach M, et al. An orthotopic model of ductal adenocarcinoma of the pancreas in severe combined immunodeficient mice representing all steps of the metastatic cascade. *Pancreas* 2001;23:227–35.
30. Schneider CA, Rasband WS, Eliceiri KW. NIH Image to ImageJ: 25 years of image analysis. *Nat Methods* 2012;9:671–5.
31. Hammer ØH, DATI, Ryan PD. PAST: paleontological statistics software package for education and data analysis. *Palaeontol Electron* 2001;4:9.
32. Lisy MR, Goermar A, Thomas C, et al. In vivo near-infrared fluorescence imaging of carcinoembryonic antigen-expressing tumor cells in mice. *Radiology* 2008;247:779–87.
33. Sato K, Watanabe R, Hanaoka H, et al. Photoimmunotherapy: comparative effectiveness of two monoclonal antibodies targeting the epidermal growth factor receptor. *Mol Oncol* 2014;8:620–32.
34. Cruz-Monserrate Z, Roland CL, Deng D, et al. Targeting pancreatic ductal adenocarcinoma acidic microenvironment. *Sci Rep* 2014;4:4410
35. Nayak TK, Garmestani K, Milenic DE, et al. HER1-targeted 86Y-panitumumab possesses superior targeting characteristics than 86Y-cetuximab for PET imaging of human malignant mesothelioma tumors xenografts. *PLoS One* 2011;6:e18198.
36. Kruwel T, Nevoltris D, Bode J, Dullin C, Baty D, Chames P, Alves F. In vivo detection of small tumour lesions by multi-pinhole SPECT applying a (99m)Tc-labelled nanobody targeting the Epidermal Growth Factor Receptor. *Sci Rep* 2016;6: 21834.
37. Wang K, Wang K, Li W, et al. Characterizing breast cancer xenograft epidermal growth factor receptor expression by using near-infrared optical imaging. *Acta Radiol* 2009;50:1095–103.
38. de Boer E, Warram JM, Tucker MD, et al. In vivo fluorescence immunohistochemistry: localization of fluorescently labeled cetuximab in squamous cell carcinomas. *Sci Rep* 2015;5: 10169.
39. Zinn KR, Korb M, Samuel S, et al. IND-directed safety and biodistribution study of intravenously injected cetuximab-IRDye800 in cynomolgus macaques. *Mol Imaging Biol* 2015;17:49–57.
40. Reagan-Shaw S, Nihal M, Ahmad N. Dose translation from animal to human studies revisited. *FASEB J* 2008;22:659–61.
41. Thurber GM, Schmidt MM, Wittrup KD. Antibody tumor penetration: transport opposed by systemic and antigen-mediated clearance. *Adv Drug Deliv Rev* 2008;60:1421–34.
42. van Driel PB, van de Giessen M, Boonstra MC, et al. Characterization and evaluation of the artemis camera for fluorescence-guided cancer surgery. *Mol Imaging Biol* 2015;17:413–23.
43. Boonstra MC, Tolner B, Schaafsma BE, et al. Preclinical evaluation of a novel CEA-targeting near-infrared fluorescent tracer delineating colorectal and pancreatic tumors. *Int J Cancer* 2015;137: 1910–20.
44. Metildi CA, Kaushal S, Pu M, et al. Fluorescence-guided surgery with a fluorophore-conjugated antibody to carcinoembryonic antigen (CEA), that highlights the tumor, improves surgical resection and increases survival in orthotopic mouse models of human pancreatic cancer. *Ann Surg Oncol* 2014;21:1405–11.
45. Metildi CA, Kaushal S, Luiken GA, et al. Advantages of fluorescence-guided laparoscopic surgery of pancreatic cancer labeled with fluorescent anti-carcinoembryonic antigen antibodies in an orthotopic mouse model. *J Am Coll Surg* 2014;219:132–41.
46. Chung CH, Mirakhur B, Chan E, et al. Cetuximab-induced anaphylaxis and IgE specific for galactose-alpha-1,3-galactose. *N Engl J Med* 2008; 358:1109–17.
47. de Geus SW, Boogerd LS, Swijnenburg RJ, et al. Selecting tumor-specific molecular targets in pancreatic adenocarcinoma: paving the way for image-guided pancreatic surgery. *Mol Imaging Biol* 2016.